FILE COPY
NO. 2

CASE FILE
COPY

TECHNICAL MEMORANDUMS

NATIONAL ADVISORY COMMITTEE FOR AERONAUTICS

THIS DOCUMENT ON LOAN FROM THE FILES OF

NATIONAL ADVISORY COMMITTEE FOR AERONAUTICS
LANGLEY AERONAUTICAL LABORATORY
LANGLEY FIELD, HAMPTON, VIRGINIA

RETURN TO THE ABOVE ADDRESS.

REQUESTS FOR PUBLICATIONS SHOULD BE ADDRESSED AS FOLLOWS:

NATIONAL ADVISORY COMMITTEE FOR AERONAUTICS
1724 F STREET, N.W.,
WASHINGTON 25, D.C.

No. 650

DEVELOPMENT OF A NON-AUTOROTATIVE AIRPLANE CAPABLE OF STEEP LANDING

By Wilhelm Schmidt

Zeitschrift für Flugtechnik und Motorluftschiffahrt
Vol. 22, Nos. 18 & 19, Sept. 28, and Oct. 14, 1931
Verlag von R. Oldenbourg, München und Berlin

FILE COPY
To be returned to the files of the National Advisory Committee for Aeronautics
Washington, D. C.

Washington
December, 1931

NATIONAL ADVISORY COMMITTEE FOR AERONAUTICS

TECHNICAL MEMORANDUM NO. 650

DEVELOPMENT OF A NON-AUTOROTATIVE AIRPLANE CAPABLE OF STEEP LANDING*

By Wilhelm Schmidt

Notation

x	path axis, tangent to the path of the C.G. of the airplane.
y	lift axis, perpendicular to path axis x and in symmetrical plane of airplane.
x y z	longitudinal axis of airplane. normal axis of airplane. lateral axis of airplane.
	All axes pass through the C.G. of the airplane; their direction is positive in the sense of the arrows of Figure 1.
$v\,(m/s)$	air speed of C.G. of airplane.
$\dot{v}\,(m/s^2)$	time rate of change of v.
$\varphi\,(o)$	gliding angle; angle between path axis x and its projection on the horizontal plane; positive, when the airplane climbs.
$\dot{\varphi}\,(1/s)$	time rate of change of φ; also rate of turning about lateral axis z, as long as this remains horizontal; positive when, viewed in the direction of positive z axis, it acts clockwise around it.
$\alpha\,(o)$	angle of attack; angle between longitudinal axis x and path axis x.

*"Beitrag zur Entwicklung eines autorotationsfreien steil landbaren Flugzeuges." Zeitschrift für Flugtechnik und Motorluftschiffahrt, Sept. 28, 1931, pp. 546-9, and Oct. 14, 1931, pp. 569-578.

$\dot{\alpha}$ (1/s) time rate of change of α; also rate of turning about lateral axis z; positive when viewed in the direction of positive z axis, acting clockwise.

Ω_x, Ω_y, Ω_z (1/s) rate of turning around the respective axis denoted by subscript; positive when clockwise, as seen in positive direction of the respective axis.

$\dot{\Omega}_z$ (1/s²) time rate of change of Ω_z.

g (m/s²) acceleration due to gravity.

γ (kg/m³) specific weight of air.

q (kg/m²) dynamic pressure $= \frac{\gamma}{2g} v^2$.

G (kg) airplane weight.

F (m²) wing area.

b (m) wing span.

t_1 (m) chord at center of wing.

t_a (m) chord at distance a from the symmetrical plane of the airplane.

a (m) distance of C.G. belonging to wing element $t_a \Delta\alpha$ from the symmetrical plane.

J_z (mkgs²) moment of inertia of airplane about lateral axis z.

F_H (m²) area of horizontal tail surfaces.

F_Q (m²) area of ailerons.

l_H (m) distance of c.p. of air load, acting on horizontal tail surfaces, from lateral axis z.

l_Q (m) distance of c.p. of air load, acting on aileron, from longitudinal axis x.

β_H (o) elevator displacement; positive downward.

$\delta_H^{(o)}$ setting of horizontal tail surfaces.

$\beta_Q^{(o)}$ aileron displacement.

The subsequent coefficients of the air loads and moments have been obtained by dividing the corresponding air loads and moments by qF (in kg) and qFt_1 (in mkg).

c_a lift; positive in positive direction of lift axis $\underline{y}_1$.

c_w drag; positive in negative direction of path axis x.

c_n normal force
c_{nQ} normal force of aileron
} positive in positive direction of normal axis $\underline{y}$.

c_t tangential force
c_{tQ} tangential force of aileron
} positive in negative direction of longitudinal axis $\underline{x}$.

c_m moment about leading edge of wing.

$\underline{M}$ moment of whole airplane
$\underline{M}_F$ moment of wing alone
$\underline{M}_H$ moment of longitudinal tail surfaces
} about normal axis $\underline{z}$

$\underline{K}$ moment
$\underline{K}_Q$ aileron moment
} about longitudinal axis $\underline{x}$

All moments are positive when opposing a positive rotation around the corresponding axis.

If the angle of attack of an airplane exceeds that for maximum lift, it no longer moves safely in the air but because of a suitable asymmetrical disturbance, shows a tendency to sideslip and to go into a spin. (Reference 1.)

This sideslip and entry into a spin is not dangerous at greater heights (references 2 and 3), but becomes exceedingly so in the vicinity of the ground. (Reference 4.)

This explains the persistent efforts which have been made for some time to make sideslip difficult. In fact, it may be prevented altogether if care is taken in the wind tunnel to prevent autorotation. (Reference 4.)

Attempts to render autorotation difficult, include: The use of so-called balancing slots on the top side of a wing, adjacent to and parallel to the leading edge, extending only over the wing tips, the corresponding slots of the left and right wing tips being connected by pipes within the wing. The rate of rotation of such a wing is lower than for an identical wing without slots (reference 5), although autorotation cannot be prevented altogether, because the compensating pipes offer resistance to the equalization of pressure, which cannot be overcome save by a pressure difference, i.e., an exisitng rotation, unless the resistance of the compensating pipes be eliminated.

Equipping an airplane wing with an auxiliary wing as wide as the main wing but with only one-third its chord, and which is adjustable around an axis parallel to the leading edge of the wing, lowers the autorotation considerably (reference 6) if the auxiliary wing is given a smaller angle of attack than the main wing. In this case the drag pertaining to low lift is comparatively great; hence the wing is unsuitable for ordinary flight. But with the auxiliary wing at a greater angle than the main wing, the total drag approximates that for the main wing alone, i.e., the wing can be used for ordinary flight also.

Experiments on a monoplane wing with sweepback have shown (reference 7) that the rate of autorotation is reduced by increasing sweepback, but at the same time it lowers the maximum lift. Autorotation did not cease entirely below a 30° sweepback. The respective maximum lift was relatively low and was comparable to that of a conventional wing with thin symmetrical profile. Such a wing is unsuited for steep landing because of the too low maximum lift, as we shall show later on.

If the wing tips are so constructed as to be rotatable as a whole, around an axis parallel to the lateral axis and can always orientate themselves in the direction of the air flow, one speaks of "floating" wing tips. If such wing tips rotate easily and are thus able to follow the least change in wind direction, there is almost com-

plete symmetry at the tips even during autorotation; hence the effect of such wing tips on autorotation is practically nil. Quite often their real purpose is something else; they are rather visualized as ailerons (reference 8), which remain effective even at great angles of attack (reference 9) and which are intended to oppose any developed autorotation. (A detailed discussion follows elsewhere.) On the other hand, designing the wing tips so that they follow any change in air flow only very gradually, may render the entry of autorotation very difficult and even prevent it altogether under certain circumstances, providing the necessary interference introduced as initial rotation is small and lasts only through a short period. Of course, it would have to be borne in mind that at the great angles of attack incidental to a steep landing, the floating wing tips would accordingly have to be just as strongly adjustable if they are to orientate themselves in the direction of the air flow.

It is generally agreed that autorotation depends primarily on the profile shape of the wing and that its occurrence is precluded when the curve of the normal force coefficient c_n pertaining to each wing element parallel to the symmetrical plane of the airplane increases continually and evenly in dependence of the angle of attack. (References 2 and 6.) The monoplane wing, to which this report is confined, has very appropriate and therefore frequently used thick, well cambered profiles, but shows, unfortunately, a very unfavorable c_n curve in this respect and is, in consequence, unsuited to prevent autorotation. Happily, the wing center does not contribute much to autorotation, so that it is only necessary to see to it that, above all, the c_n curve for the wing tips increases as nearly as possible consistently and uniformly, while the center of the wing may, to ensure a high total lift, be given a thick, pronounced camber.

In the following we develop a non-autorotating monoplane wing. The conditions imposed on such a wing, aside from its freedom from autorotation, with respect to its polars and its construction, are taken into account as far as possible.

It is indicated that the autorotation characteristics of a wing are dependent upon the speed of air flow (reference 10) as well as on the angle of yaw. (Reference 7.) At the beginning of sideslip, which is almost synonomous

with autorotation, and with which we are concerned here, the angle of yaw is small (reference 4), so that it may be disregarded for the present. The change in autorotation properties induced by a change in wind velocity is likewise of a finer type and therefore ignored. Upon elimination of autorotation and, through it, the danger of sideslip, the airplane can be flown at a great angle of attack by using a special control, and likewise be landed at a very steep angle, to reduce the landing run.

The present investigation postulates the knowledge of the behavior of certain conventional wings of different chords and cambers with respect to their air loads at large angles of attack. This, in particular, applies to the curve of the normal force coefficient c_n with respect to the angle of attack, and to which we subsequently refer briefly as the c_n curve. Since the data on this c_n curve at angles up to $\alpha = 90^\circ$ were limited to very few wings, the already available (reference 11,a) data up to 20° were supplemented by the measurements on a large number of conventional wing sections with Joukowski profile, and in particular for four typical wings (fig. 2) with different thickness/camber ratio (d/f) to the approximately half chord l. Thickness and camber are explained in reference 11,b. The tests, conducted in the Göttingen wind tunnel at 31 m/s (101.7 ft./sec.) wind velocity, range over $\alpha = 20^\circ$ to $\alpha = 50^\circ$. Since at large angles the air loads on conventional wings show no essential difference from one another and measurements beyond 50° would have entailed a rearrangement of the models, we stopped at 50° and compared the air loads for angles beyond 50° with those of wings already tested. The measurements included lift, drag and moment around the leading edge, as shown in Figures 3-6, along with the computed normal force coefficient plotted against α. The thinner and flatter the profile the better the continual rise of the c_n curves.

Test Wing No 1

The wing tips in Figure 7 evince, in order to prevent autorotation, an appropriately thin, symmetrical profile gradually merging into a thick, heavily cambered high lift section toward the center of the wing. All profile chords are parallel to one another. Later, I learned that a similar wing, although designed for different purposes, has been described elsewhere. (Reference 12.)

To evaluate the autorotation characteristics of a wing one merely needs to know the moments about the longitudinal axis set up by a rotation around the path axis, which is a comparatively easy matter. Through cuts parallel to the symmetrical axis of the airplane the wing is divided into a number of components having a C.G. distance a from the symmetrical plane, a span Δa, and a constant chord t_a with, in addition, constant profile. The $K\Omega_x$ coefficient of the moment about the longitudinal axis introduced by a rotation Ω_x about the path axis is

$$\left.\begin{aligned} K_{\Omega x} &= \frac{1}{Ft_1} \Sigma c_{n_a} \frac{1}{\cos^2 \Delta\alpha} t_a \, a \, \Delta a \\ \text{with} \quad \Delta\alpha &= \arctan \frac{a\,\Omega_x}{v} \end{aligned}\right\} \qquad (1)$$

and c_{n_a} as coefficient of the normal force for one component. This varies along the wing span and can be defined as approximately equal to the coefficient of a normal wing with corresponding profile. Of these, profiles 3 to 7, in Figure 2, are very much alike, so that the corresponding normal force coefficients may be taken from Figures 3-6. The normal force coefficient for profiles 1 and 2 was assimilated to the others.

Figure 8 shows coefficient $K\Omega_x$ of the calculated moments about the longitudinal axis plotted against $\frac{b\Omega_x}{2v}$ with angle of attack as parameter. The corresponding wind-tunnel data are given in Figure 9. They were directly measured as moments about the longitudinal axis, thus obviating extrapolation. The air speed was 30 m/s (98.4 ft./sec.). Figure 10 depicts the wing mounted on a novel moment balance in the Göttingen wind tunnel. A comparison of the computed with the experimental figures revealed the shape of the curves in fairly good agreement, but of less satisfactory accord in absolute values. Whereas, theoretically, only positive moments occur, i.e., moments opposing a positive rotation, debarring entry of autorotation, experimentally, negative moments are always present which accelerate an incipient rotation and facilitate autorotation.

Figure 11 discloses the coefficients of lift, drag, and moment around the leading edge of the wing plotted against the angle of attack as obtained at 30 m/s air speed.

In addition to the wing polars with progressively varying profile over the span, Figure 12 also shows the wing polar for the Junkers A 35 type low monoplane wing. At the low lift of ordinary flight the drag of the tested wing was considerably greater than that of the other. Although the wing drag itself is only a third of that of the whole airplane, we shall strive nevertheless to reduce the comparatively high drag for low lift, which is due to the still unfavorable distribution of lift over the span. (Fig. 13.) Because of this lift distribution there is introduced an additional flow in the direction of the lateral axis which sets up violent eddies over a large portion of the span, such as occur only at the tips of a wing with constant profile, thus making a high drag inevitable. The formation of such eddies may be reduced by making provisions, as shown, that no additional flow in the direction of the lateral axis can occur.

Normal Force of a Wing with Thin, Symmetrical Profile of a Flat Plate and of a Lattice

In addition to the above-mentioned thin, symmetrical section, we further examined several others which are particularly well suited to render autorotation difficult.

Figure 14 shows the normal force coefficient for a normal wing with the thin, symmetrical Göttingen normal profile No. 537 plotted against the angle of attack, and besides, the c_n curves (reference 14) for flat plates with different aspect ratio. It is seen that the flat plate and the thin profile, as regards their c_n curve, can be interpreted as approximately equivalent; that, moreover, the respective c_n curve is materially influenced by aspect ratio t:b and shows an almost consistent rise up to about $\alpha = 90^\circ$ only when $t:b < 1:5$. It is far removed from the desired uniform rise.

By dividing a wing with thin symmetrical profile through cuts parallel to the leading edge, into an uneven number of identical parts and then removing those that are even-numbered, we obtain a wing somewhat as seen in Figure 15, which may be called a thin, symmetrical perforated profile. Such a wing is very much like a lattice. In Figure 14 a part of the profile belonging to a rectan-

gular lattice of about 1 m (3.28 ft.) thickness, and 0.5 m (1.64 ft.) width is plotted, along with the normal force coefficient against the angle of attack, the total surface being used as reference surface. (Reference 15.)

At small α the normal force of the lattice is about equal to half of that of the corresponding flat plate of the same aspect ratio, because the supporting surface is only about half as large, which, in fact, agrees very closely with the theory. (Reference 13,b.) The closer the angle of attack approaches that of 90°, the more the gaps appear to be filled in, until at 90° the total surface may be looked upon as supporting surface.

A similar, though not quite as steadily rising c_n curve is ostensibly obtained with a wing of very thin, symmetrical profile, whose top surface has been roughened. Experiments are not available as yet respecting this.

Experiments on a Handley Page wing with interceptor (slotted airfoil plus interceptor) have shown (reference 16) that the respective c_n curve rises steadily up to about $\alpha = 90°$, even if not quite as uniformly as that of the lattice. The actuation of the Handley Page device postpones, as we all know, the separation of the flow for higher angles of attack, and in that manner assures a powerful action of the ailerons even at large α. For this reason the Handley Page device is frequently mounted at the wing tips. The corresponding c_n curve at first rises to a high maximum lift, and then drops suddenly and, of necessity, considerably. As a result, it therefore differs very materially from the desired shape of continuous rise stipulated to reduce autorotation. As soon as the angle of attack exceeds the value for maximum lift of the wing tips, the wing must accordingly autorotate violently. To oppose this is the purpose of the interceptors. By its actuation the flow on the upper side of the wing is made to separate even at small α, hence the effect of the Handley Page device is made retrogressive. In that way the c_n curve of the wing tips assumes the desired steady rise, i.e., the wing tips oppose autorotation. It is readily agreed that such a mechanism is extremely complicated. Another point to be borne in mind is that through the actuation of the interceptor the powerful effect of the ailerons at large angles of attack is, of course, lost. (See Appendix.)

Test Wing No. 2

The wing is shown in Figure 16. It consists of a center portion with thick, well cambered profile, equipped with the Handley Page device for raising the maximum lift without affecting the autorotation very materially. Next to the central part is another with thin, symmetrical profile. The extreme wing portions have a thin, symmetrical perforated profile to prevent autorotation as much as possible. All parts with different profile are separated from one another by plates to ensure lower drag at low lift.

The wing was tested 30 m/s wind speed in the Göttingen tunnel.

As long as the slot was closed and the flap not set, the polar of this wing, at low lift, coincided with that of a low wing of the Junkers A 35 type, as expected, and as seen in Figure 17. Consequently, the wing can be used for ordinary flight. Operating the Handley Page device, i.e., changing the slot setting and turning the flap downward raises, according to Figure 18, the maximum lift to higher angles α.

The lift coefficient is estimated as:

$$c_a = \frac{F_1}{F} c_{a_1} + \frac{F_2}{F} c_{a_2} + \frac{F_3}{F} c_{a_3} \qquad (2)$$

where F, F_1, F_2 and F_3 denote the area of the whole wing, that is, of the central part, the two adjacent pieces and the two pieces at the tips, and c_a, c_{a_1}, c_{a_2}, and c_{a_3} the respective lift coefficients. The drag coefficient of the whole wing can be defined in the same manner.

For the case of closed slot and flaps, the coefficients c_{a_1} and c_{w_1} for the middle portions can be taken from Figure 4. The c_{a_2} and c_{w_2}; as well as c_{a_3} and c_{w_3} coefficients are approximately like those in Figures 6, and 19, respectively. According to Figure 18, the c_a and c_w coefficients for the whole wing deduced from equation (2), are in very close accord with those obtained by experiment.

The moment about the leading edge of the wing presents no unusual feature. The moment about the longitudinal axis was calculated according to equation (1), and specifically, with slot open and flap turned down. We determined the unknown normal force coefficient for the middle portion with adjustable Handley Page mechanism, using the corresponding values in Figures 6 and 19, according to equation (2). Figure 20 shows the $K\Omega_x$ coefficient, defined according to (1), of the moment about the longitudinal axis produced by a rotation Ω_x about the path axis, plotted against $\frac{b\Omega_x}{2v}$ with α as parameter. Granted even that these strong positive moments, according to calculation, should in reality be a little less strongly positive, one can nevertheless presume that they always remain positive, so that no autorotation can occur. As a matter of fact, experiments in the Göttingen wind tunnel have shown that the wing with adjusted Handley Page mechanism does not autorotate even at such large angles as $\alpha = 40^\circ$, and beyond this no autorotation is to be expected. The autorotation set-up of this second wing is shown in Figure 21.

Test Wing No. 3

The drag for low lift can also be reduced by placing the zero lift axes of all profiles into one plane. Of course, this is merely a measure to influence the polars of the wing. Its autorotation characteristics are little affected by it, since they are already primarily decided by the shape of the wing tips.

Figure 22 presents this third wing with symmetrical perforated profile at the tips, gradually developing into a thick, heavily cambered section in the center, whereby the zero lift lines of all modified Joukowski profiles lie in one plane. For structural reasons the wing tips were kept comparatively thick, in order to be able to turn them as a whole, if necessary, like ailerons around an axis transverse to the flight direction. To insure, in addition, a minimum influence, particularly by aileron displacement, through the adjacent part, they were separated by plates.

We tested this wing at 30 m/s in the Göttingen wind tunnel.

The drag of the middle portion with plates for low lift is, according to Figure 23, about equivalent to that of a Junkers A 35 monoplane wing and becomes, when adding the thick ailerons of Figure 22, materially greater. The lift curve in both cases has, according to Figure 24, a maximum which, as shown later, is high enough for steep landing. Contrary to expectation, the wing did autorotate even if only very little.

Roughening the top side of the wing between the third and fourth ribs by a coating of fine sand, the wing autorotates more feebly. This apparently confirms our conjecture voiced in a previous paragraph according to which the respective c_n curve of a wing with very thin, symmetrical profile and roughened top side rises similarly even if not so consistently uniform as that of the lattice. But even with this it was impossible to make the wing altogether non-autorotative.

After searching investigations it was concluded that the cause of this unexpected slight autorotation lies in the wing tips with comparatively thick profile. Subsequent tests made after substituting the tips sketched in Figure 25, revealed that the wing cannot be made to autorotate on any condition. Every rotation, no matter how strong, is immediately and vigorously damped out and the wing comes quickly to rest. Figure 26 shows the completely non-autorotating wing mounted in the Gottingen wind tunnel.

Thus it is seen that it is possible to design an absolutely non-autorotating monoplane wing merely by a correct selection of profiles without other additional aids.

The drag of the monoplane wing, according to Figure 25, is most probably lower than that of the wing with thin tips in Figure 22, the polars of which are given in Figure 23. The respective maximum lift can, rather, be assumed greater than indicated in Figure 24.

Aside from the material improvement in the wing polars of the non-autorotating monoplane wing by an ingeniously contrived choice of profiles, it is also possible to make such a wing satisfy fully all the conditions which may be laid down for its polars. The constructional aspects of the wing tips will be fully discussed in a subsequent chapter.

Control of the Non-autorotating Airplane

In order that a non-autorotating airplane may be flown at high angles of attack and, as we will show, be capable of steep landing, it must, first of all, have horizontal tail surfaces which ensure a balance of the moments around the lateral axis even at angles of attack beyond those for lift maximum.

Figure 27 shows the coefficients $\underline{M}$, $\underline{M}_F$, and $\underline{M}_H$ of the airplane wing and horizontal tail surface moments, respectively, around the lateral axis for a low-wing monoplane of the Junkers A 35 type. Since the horizontal tail surface moment varies comparatively little, as a rule, even with extreme elevator displacement, a balance of the moments about the lateral axis in the orthodox airplanes of to-day is possible only up to an angle of attack which is in the neighborhood of that for maximum lift.

Moving the whole horizontal tail group through angle δ_H around an axis parallel to the lateral axis, changes the angle of attack of the horizontal tail group by a like amount, the curve of its $\underline{M}_H$ moment in Figure 27 is moved by this amount δ_H parallel to the ordinate. In this manner a balance of the moments around the lateral axis is ensured even at arbitrarily large angles of attack.

In order to retain the effectiveness of a rudder displacement even at large α, it is recommended to desist from covering the elevator clear up to the fuselage. (Reference 3.)

An aileron displacement generally results in asymmetry at both wing tips, thereby changing the autorotation characteristics. It sets up, aside from the desired moment about the longitudinal axis, an undesirable moment about the normal axis, which nullifies in part the effect intended, particularly at large angles of attack.

Such ailerons, that is, the conventional type of to-day, including the Handley Page aileron flaps, are dismissed from further consideration and we confine ourselves to an ideal aileron, the displacement of which does not alter the autorotation characteristics of the wing and sets up a vigorous moment about the longitudinal axis without an unwelcome moment about the normal axis.

To ensure the same autorotative properties of the wing with aileron displacement, the profile of the wing tips must be retained even when the aileron is displaced, i.e., the wing tips must be rotatable as one unit around an axis transverse to the direction of flight, similar to the ailerons illustrated in Figures 16, 22, and 23.

With β_Q = aileron displacement, F_Q = area of aileron, l_Q = distance of the C.G. of the applied air load from the axis of the fuselage, and $c_{n_Q}(\alpha + \beta_Q)$ and $c_{n_Q}(\alpha - \beta_Q)$ as the corresponding coefficient of the normal force; the coefficient of the aileron moment about the longitudinal axis is:

$$K_Q = \frac{2 F_Q l_Q}{F t_1} [c_{n_Q}(\alpha + \beta_Q) - c_{n_Q}(\alpha - \beta_Q)] \qquad (3)$$

By fixed $\frac{F_Q l_Q}{F t_1}$ this factor is constant for the angles of attack under consideration here, if

$$c_{n_Q}(\alpha + \beta_Q) - c_{n_Q}(\alpha - \beta_Q)$$

is constant for this.

Such a stipulation can be complied with, for example, by using floating ailerons with suitable symmetrical profile to ensure a symmetrical c_n curve with respect to zero position. For symmetrical reasons no undesirable moment about the normal axis can occur.

The same result can also be achieved by using ailerons which do not need to orientate themselves into the particular direction of the air stream, thus being more simple from the point of view of construction. To keep the moment about the longitudinal axis as constant as possible within the angles of attack in question, and to render the moment about the normal axis evanescently small, the difference of the normal forces $c_{n_Q}(\alpha + \beta_Q) - c_{n_Q}(\alpha - \beta_Q)$ must, according to equation (3) be as constant as possible, or in other words, the c_n curve of the wing tips within this range must rise consistently and uniformly. In addition, the corresponding difference of the tangential forces $c_{t_Q}(\alpha + \beta_Q) - c_{t_Q}(\alpha - \beta_Q)$ must disap-

pear as nearly as possible, i.e., the tangential force of the wing tips in this range must be as constant as possible. Figure 19 shows that the lattice fulfills these conditions very satisfactorily. Consequently, it can be presumed that the ailerons of the third investigated, completely non-autorotating monoplane wing, in Figure 25, satisfy the above stipulations:

Aileron displacement scarcely changes the autorotating properties. Aileron displacement supplies, even at large angles of attack, a strong moment about the longitudinal but without an undesirable moment about the normal axis.

The outer form of the ailerons has practically no effect on it. Thus, to simplify construction, it is better to use an aileron of smaller width but greater chord. The design of the floating ailerons on the Curtiss Tanager (reference 8) demonstrated that the constructional difficulties are not insuperable.

Steep Landing of the Non-autorotating Airplane

Whereas the engine power may under certain circumstances affect the power flight, that is, render a comparatively steep start possible by sufficiently high engine power, in glide flight the engine is stopped, the propeller thrust is practically zero, so that, for example, the glide angle φ and the rate of glide v of an airplane descending in steady, level flight is dependent only on the angle of attack α. Figure 28 shows the peculiar course of v and φ plotted against α for the present-day types of airplanes. According to it a large glide angle is obtainable in two ways: one, by small α and large v, that is, in a dive; the other, at angles α beyond those for maximum lift and small v. If the horizontal tail group in the conventional practice of to-day is designed to ensure a balance of the moments about the lateral axis, at the highest, at an angle α near to that for stalling, the pilot is unable to force a steady glide at greater angles of attack, i.e., force a steep glide by low rate of glide, even though the airplane were equipped with slotted wings. But, since the steep glide at low v for large angles of attack is preeminently suited, as we will show, for steep landing and, thus, shorter taxying run, it

should be attempted to make accessible for steep landing the range of large angles of attack, hitherto dreaded because of the danger of nosing over.

This is accomplished by the above design of the completely non-autorotating monoplane wing.

An airplane equipped with such a wing can, by using the above-described longitudinal tail surfaces, be flown at very high angles of attack and be put into a very steep glide without going into a sideslip and into a spin as heretofore.

In the absence of a specially designed landing gear a steep landing is possible only when the pilot is able to reduce the inclination of the fuselage to the path, i.e., angle α, and at the same time change the steep path of the C.G. of the airplane into one almost parallel to the ground, so that the fuselage, even in steep landing, assumes the slope for the usual landing directly before touching the ground. That is to be decided by integration of the basic equations for level glide without side wind, where we introduce a temporarily variable horizontal tail surface displacement. The equations read:

$$\dot{v} = - g \sin \varphi - \frac{\gamma}{2} \frac{F}{G} v^2 c_w \tag{4}$$

$$\dot{\varphi} = - g \frac{\cos \varphi}{v} + \frac{\gamma}{2} \frac{F}{G} v c_a \tag{5}$$

$$\dot{\Omega}_{\underline{z}} = - \frac{\gamma F t_1}{2g J_{\underline{z}}} v^2 \underline{M} \tag{6}$$

where

$$\Omega_{\underline{z}} = \dot{\alpha} + \dot{\varphi} \tag{7}$$

They can be simplified considerably by reason of the following assumptions:

1. Figure 29 shows that as in all such experiments, so here also, the air speed v is constant during the time in question, thus eliminating equation (4).

2. The slightly changing value $\cos \varphi$ within the range considered is substituted by $\cos \varphi_o$ constant.

3. Lift coefficient c_a is dependent only on α. The $c_a = f(\alpha)$ curve is assimilated to a straight line for the pertinent angles α conformably to Figure 30, so that:

$$c_a = m_1 \alpha + n_1 .$$

4. The change in α_H for the horizontal tail group, as a result of only a slight rotation Ω_Z about the lateral axis is:

$$\Delta\alpha_H = \frac{l_H}{v} \Omega_Z$$

5. As long as there is no rotation about the lateral axis the coefficient of the horizontal tail surface moment M_H depends only on the angle of attack α. The $M_H = f(\alpha)$ curve is assimilated to a straight line (fig. 27) as follows:

$$M_H = m_2 \alpha + n_2 .$$

A displacement of the horizontal tail group shifts this straight line parallel to itself, thus changing n_2 only. This displacement is not accomplished suddenly, but for reasons (which will be analyzed in a subsequent section) and in support of facts, according to the following law:

$$n_2 = U + Ve^{-kt} ,$$

that is, the pilot displaces the horizontal tail surfaces first quickly, then more slowly. A rotation Ω_Z about the lateral axis introduced by this displacement changes only the angle of attack α_H and through it the coefficient of horizontal tail surface moment M_H by the amount

$$m_2 \frac{l_H}{v} \Omega_Z .$$

The curve of the coefficient of the wing moment M_F about the lateral axis with respect to α is conformably to Figure 27 assimilated to a straight line for the pertinent range of angles α as follows:

$$M_F = m_3 \alpha + n_3 .$$

Now the moment coefficient M about the lateral axis is:

$$\underline{M} = (m_2 + m_3)\,\alpha + n_3 + U + Ve^{-kt} + m_2 \frac{l_H}{v}\,\Omega_{\underline{Z}} \qquad (8)$$

We disregard the term $m_2 \frac{l_H}{v}\,\Omega_{\underline{Z}}$, which is small as compared to the others and define U and V from equation (8) as follows: At time-interval $t = 0$ the initial equilibrium position α_0 reveals:

$$\underline{M} = 0 = (m_2 + m_3)\,\alpha_0 + n_3 + U + V$$

For α_0', we find:

$$\underline{M} = 0 = (m_2 + m_3)\,\alpha_0' + n_3 + U.$$

Consequently,

$$U = -(m_2 + m_3)\,\alpha_0' - n_3$$

$$V = (m_2 + m_3)\,(\alpha_0' - \alpha_0).$$

Now the modified equations (4 to 7) read as:

$$\dot{\varphi} = a_1\,\alpha + b_1 \qquad (9)$$

$$\dot{\Omega}_{\underline{Z}} = a_2\,\alpha + b_2 + c_2\,e^{-kt} + d_2\,\Omega_{\underline{Z}} \qquad (10)$$

$$\Omega_{\underline{Z}} = \dot{\alpha} + \dot{\varphi} \qquad (11)$$

Herein,

$$a_1 = \frac{\gamma\, v\, F}{2\, G}\, m_1$$

$$b_1 = \frac{\gamma\, v\, F}{2\, G}\, n_1 - \frac{g}{v} \cos \varphi_0$$

$$a_2 = -\frac{\gamma\, v^2 F\, t_1}{2\, g\, J_{\underline{Z}}}\,(m_2 + m_3)$$

$$b_2 = -\frac{\gamma\, v^2\, F\, t_1}{2\, g\, J_{\underline{Z}}}\,(U + n_3)$$

$$c_2 = -\frac{\gamma\, v^2\, F\, t_1}{2\, g\, J_{\underline{Z}}}\, V$$

$$d_2 = -\frac{\gamma\, v\, l_H\, F\, t_1}{2\, g\, J_{\underline{Z}}}\, m_2.$$

By inserting the nonhomogeneous differential equation of the second order,

$$\ddot{\alpha} + (a_1 - d_2)\,\dot{\alpha} - (a_1\,d_2 + a_2)\,\alpha = c_2 e^{-kt} + b_1\,d_2 + b_2$$

we obtain from equations (9) to (11):

$$\alpha = A_1\,e^{\delta t}\,\sin\,(\zeta_1 + \epsilon\,t) + B_1\,e^{-kt} + C_1 \qquad (12)$$

Herein

$$\delta = -\frac{a_1 - d_2}{2}$$

$$\epsilon = \sqrt{-\delta^2 - a_1\,d_2 - a_2}$$

$$C_1 = -\frac{b_1\,d_2 + b_2}{a_1\,d_2 + a_2}$$

$$B_1 = \frac{C_2}{k^2 - (a_1 - d_2)\,k - a_1\,d_2 - a_2}$$

$$\zeta_1 = \arctan\frac{\epsilon\,(\alpha_0 - B_1 - C_1)}{\dot{\alpha}_0 - \delta\,(\alpha_0 - B_1 - C_1) + k\,B_1}$$

$$A_1 = \frac{\alpha_0 - B_1 - C_1}{\sin\,\zeta_1}$$

Equations (9) and (11) further yield:

$$\varphi = A_2\,e^{\delta t}\,\sin\,(\zeta_2 + \epsilon\,t) + B_2\,e^{-kt} + C_2 + D_2\,t \qquad (13)$$

$$\Omega_z = A_2\,e^{\delta t}\,\sin\,(\zeta_3 + \epsilon t) + B_3\,e^{-kt} + C_3 \qquad (14)$$

Herein,

$$A_2 = \frac{a_1\,A_1}{\sqrt{\delta^2 + \epsilon^2}}$$

$$\zeta_2 = \zeta_1 - \arctan\frac{\epsilon}{\delta}$$

$$B_2 = -\frac{a_1\,B_1}{k}$$

$$D_2 = a_1\,C_1 + b_1$$

$$C_2 = \varphi_0 - A_2 \sin \zeta_2 - B_2$$

$$A_3 = A_1 \sqrt{(a_1 + \delta)^2 + \epsilon^2}$$

$$\zeta_3 = \zeta_1 + \arctan \frac{\epsilon}{\delta + a_1}$$

$$B_3 = (a_1 - k) B_1$$

$$C_3 = D_2.$$

Using the final figures for a monoplane of the Junkers A 35 type as basis, we calculated the course of α, φ and Ω_z according to equations (12) to (14) as it occurs as a result of a disturbance of the initial position for steep glide introduced by progressive elevator displacement (forward up to stalling). The figures for the initial attitude are:

$$\gamma = 1.20 \text{ kg/m}^3$$

$$\alpha_0 = 28^\circ$$

$$\dot{\alpha}_0 = 0$$

$$c_{a_0} = 0.99 \quad m_1 = -2.12 \quad n_1 = 2.03$$

$$c_{w_0} = 0.53$$

$$\varphi_0 = -28.2^\circ$$

$$\dot{\varphi}_0 = 0$$

$$v = 28.0 \text{ m/s}$$

$$m_2 = 0.870$$

$$U = -0.241$$

$$V = -0.211$$

$$k = -1$$

$$m_3 = 0.230$$

$$n_3 = -0.085$$

In Figure 31 the angle of attack and of glide, in addition to the rate of rotation about the lateral axis are shown plotted against the time.

The angle of attack essentially changes according to the same exponential function e^{-kt}, conformably to which the displacement occurs. This exponential function is superposed by an evanescent vibration whose amplitude A is governed by the violence of the forward displacement. If very abrupt, it introduces a violent vibration around the originally fairly constant equilibrium position. On the other hand, a very gradual forward displacement forces the angle of attack very slowly into the new equilibrium position with practically no perceptible vibrations. The angle of attack scarcely assumes a value lower than that for maximum lift, so that assimilation of the lift curve to a straight line (i.e., the previous solution of the basic equation) is possible, according to Figure 30, within the stipulated range of α.

Resorting to a likewise gradual elevator displacement, we disturbed the same initial position of equilibrium as above, and then calculated the time rate of change of the variables by numerically integrating equations (4) to (7). According to Figure 29, the introduced vibration is so violent that the maximum lift is exceeded and the previously applied assimilated straight of the lift curve is relinquished. For this reason the vibrations are more slowly damped out than in the other example. But even so the principle is maintained: the angle of attack gradually changes over into the new equilibrium position in correspondence with the gradual elevator displacement. After a short time even the change of the glide angle assumes an approximately constant value which, according to equation (13) is essentially equal to D_2.

This D_2 is of great significance for the landing:

$$D_2 = \frac{v(c_{a_0}' - c_{a_0})}{\frac{2\,G}{\gamma\,F} + l_H \frac{m_1\,m_2}{m_2 + m_3}}.$$

As a rule, $l_H \frac{m_1 m_2}{m_2 + m_3}$ may be disregarded with respect to $\frac{2}{\gamma} \frac{G}{F}$, so that,

$$D_2 = \frac{\gamma}{2} v \frac{F}{G} (c_{a_0}' - c_{a_0}),$$

or, in other words, the direction of the path of the C.G. of the airplane can be changed that much quicker:

1. The greater the air speed v of the C.G. of the airplane;

2. The smaller the wing loading $\frac{G}{F}$;

3. The greater the difference $c_{a_0}' - c_{a_0}$ between lift coefficient c_{a_0}' for the new equilibrium position α_0' and the coefficient c_{a_0} for the initial equilibrium position α_0.

Therefore, the prospect of steep landing is confined to airplanes whose lift curve has a high enough maximum and after that drops steeply enough and within a sufficiently large range of angles of attack. For such the direction of the path can be changed just as quickly into a steep glide as into the hitherto usual flat glide. As concerns the reversal of the path when landing, it is utterly immaterial whether the pilot pulls the controls at small angles of attack or whether he pushes them at large angles α. The unusual feature is that in a steep glide he must displace the controls forward if he wants to raise the path.

After some time the glide angle becomes positive, according to Figure 31; that is, the airplane climbs, which was not at all contemplated. This climb can be counteracted by continuing the forward displacement, so that the airplane assumes an angle of attack below that for maximum lift, after which the lift and the path drops. In this manner a reversal of the path into one parallel to the ground can be obtained. The time rate of change in angle of attack and of glide during such a landing maneuver is shown in Figure 31. The initial equilibrium position is characterized by a large angle of attack and of glide. At first the airplane is gradually pushed until it has nearly reached the angle for maximum lift. Because

of the transition to smaller angles α and consequently greater lift, the path rises very quickly. After awhile the airplane is pushed still further, the angle of attack becomes still smaller, whence the lift drops as soon as the value for maximum lift has been exceeded. The flight path would drop also but for the tendency of the airplane to climb. The reversal of the path in consequence is only reduced at first until it finally ceases altogether. In the present case this takes from about 5 to 6 seconds, according to Figure 31.

Referring to Figure 32, we find the height of landing, plotted against the landing distance s for a normal as well as for a steep landing of a monoplane of the Junkers A 35 type. In a normal landing the glide angle is about 6° to 7°. It requires about 300 m (985 ft.) to land from a height of around 40 m (130 ft.). In the steep landing the airplane can be set down much sooner. Since the corresponding landing speed as well as the glide angle and thereby the landing distance are virtually the same in both cases, the steep landing presents a saving of about 200 m (656 ft.) in taxying run, when the airplane must land over a 40 m (131 ft.) high obstacle.

Appendix

The consideration regarding the effect of the Handley Page device is based upon the assumption that both interceptors can be operated independently from the actuation of the ailerons, as soon as the airplane approaches the stalling angle. This also explains the conclusion that any aileron deflection must be ineffective at large angles of attack.

According to the information given me by Dr. Lachmann, the interceptors are coupled to the ailerons in such a way that aileron displacement is simultaneously followed by a different setting of one of the interceptors. The interceptors are not, as I assumed, a stabilizing, but rather a control mechanism. By actuating the ailerons and thereby one of the interceptors, an adequately strong aileron moment is obtained even at large angles of attack, by which any existing autorotation even if violent, can be made to cease.

The relatively strong aileron moment is caused solely by the actuation of one of the interceptors. Thus, the same effect might be obtained if the actuation of the aileron were separate from that of the interceptor, as I assumed in my report. Even then the interceptor would remain like the aileron, a control mechanism. Besides, it could act as stabilizing device, either automatic or controllable by the pilot, for the purpose of steep landing, as soon as the airplane approaches the dangerous large angle of attack. Thus the interceptor could serve a twofold purpose - control and stabilization.

The fundamental difference between wing tips equipped with interceptors and my proposed design of wing tips with perforated profile formed as ailerons, is that it prevents the formative stage of autorotation, i.e., sideslipping, even at the very high angles of attack necessary for steep landing, without requiring any supplementary device, automatic or manipulated by the pilot.

Translation by J. Vanier,
National Advisory Committee
for Aeronautics.

References

1. Baranoff, A. v., and Hopf, L.: Combined Pitching and Yawing Motion of Airplanes. Luftfahrtforschung, March 20, 1929. T.M. No. 620, N.A.C.A., 1931.

2. Fuchs, Richard, and Schmidt, Wilhelm: The Steady Spin. Luftfahrtforschung, Feb. 27, 1929. T.M. No. 630, N.A.C.A., 1931.

3. Fuchs, Richard, and Schmidt, Wilhelm: The Dangerous Flat Spin and the Factors Affecting It. T.M. No. 629, N.A.C.A., 1931.

4. Fuchs, Richard, and Schmidt, Wilhelm: The Dangerous Sideslip of a Stalled Airplane and Its Prevention. Z.F.M., July 14, 1931. T.M. No. 638, N.A.C.A., 1931.

5. Schrenk, O.: A Possible Method for Preventing the Autorotation of Airplane Wings. Z.F.M., Nov. 14, 1929. T.M. No. 569, N.A.C.A., 1930.

6. Fuchs, Richard, and Schmidt, Wilhelm: Air Forces and Air-Force Moments at Large Angles of Attack and How They are Affected by the Shape of the Wing. Z.F.M., Jan. 14, 1930. T.M. No. 573, N.A.C.A., 1930.

7. Ober, Shatswell: Some Experiments on Autorotation of an Airfoil. T.N. No. 319, N.A.C.A., 1929.

8. Crofoot, A. B.: Curtiss Tanager, Judged the Safest Aircraft in Guggenheim Contest, was Designed to Meet Production Requirements with Few Changes. Automotive Industries, Jan. 18, 1930.

9. Knight, Montgomery, and Bamber, Millard J.: Wind Tunnel Tests on a Model of a Monoplane Wing with Floating Ailerons. T.N. No. 316, N.A.C.A., 1929.

10. Anderlik, E.: Experiments on Autorotation. Z.F.M., August 28, 1926. T.M. No. 380, N.A.C.A., 1926.

References (continued)

11. Prandtl, L., and Betz, A.: Report of the Aerodynamical Research Laboratory at Gottingen, No. 3, 1927. Verl. R. Oldenbourg, Munchen und Berlin.
a) Measurements on Joukowski Profiles, III 3.
b) Theories on Joukowski Profiles, I 4.
c) Wind Screens, III 21.

12. Lippisch, A.: Experiments with New Airplane Types. Report of the R.R.G. Research Institute. Z.F.M., June 28, 1928.

13. Fuchs, Richard, Hopf, Dr., and Ludwig, Dr.: Aerodynamik. Part I. Air Forces. Part II. Motion of Aircraft. Verl. R. G. Schmidt & Co., Berlin W. 62, 1922.

14. Föppl, O.: Wind Forces on Flat and Curved Plates. Diss. Tech. Hochschule Aachen, 1911. Verl. J. Springer, Berlin.

15. Pirath, C.: Experiments for the Determination of the Best Design for Windbreaks for Switch Terminals. Verkehrstechnische Woche, Vol. 24, No. 9, Feb. 26, 1930.

16. Stevens, H. L.: Testing Aeroplane Controls. The Journal of the Royal Aeronautical Society, No. 242, Vol. 35, Feb., 1931.

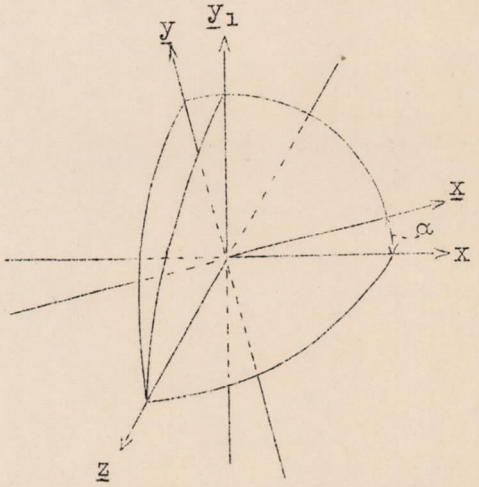
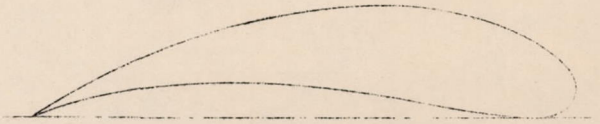


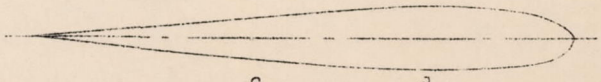
Fig.1 Definition of symbols.



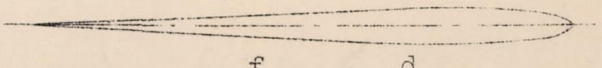
Göttingen 577, $\frac{f}{l}$ =0.200 $\frac{d}{l}$ = 0.150



Göttingen 580, $\frac{f}{l}$ = 0.100 $\frac{d}{l}$ = 0.100



Göttingen 429, $\frac{f}{l}$ = 0 $\frac{d}{l}$ 0.100



Göttingen 537, $\frac{f}{l}$ = 0 $\frac{d}{l}$ = 0.050

Fig.2 Profiles of tested wings.

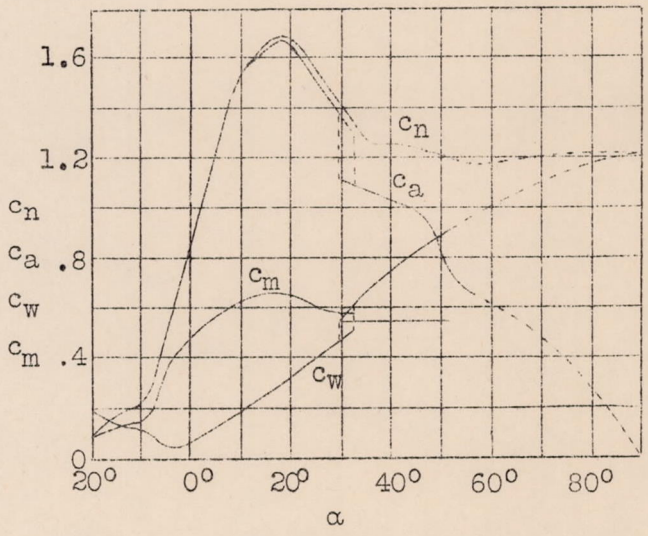
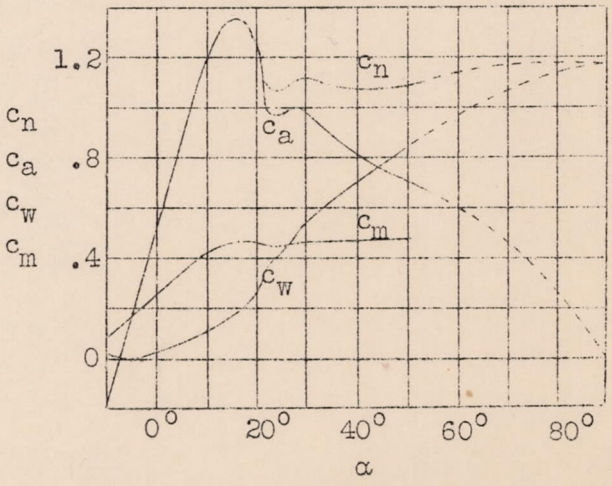


Fig.3 Göttingen 577



Fig,4 Göttingen 580

Lift coefficient,drag coefficient and moment about leading edge, also of normal force plotted against α for a conventional wing having a profile conformably to Fig.2

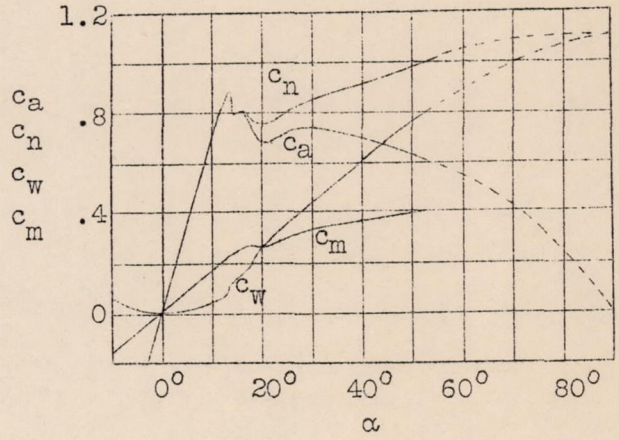


Fig.5 Göttingen 429

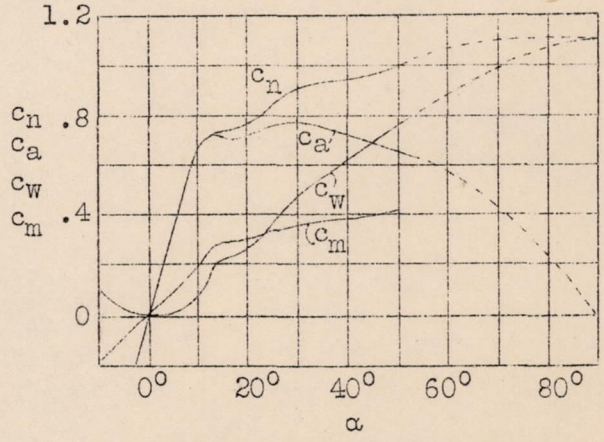
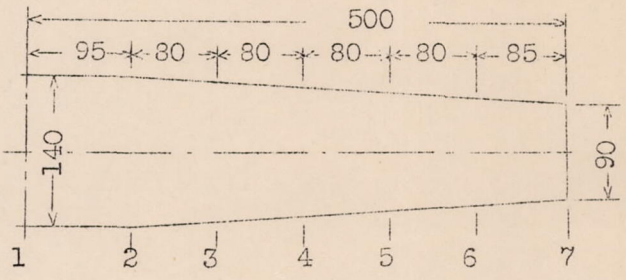
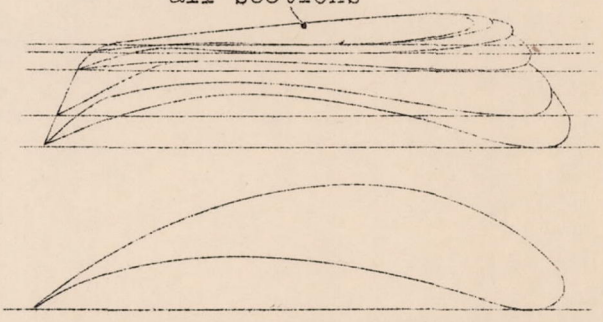


Fig.6 Göttingen 537

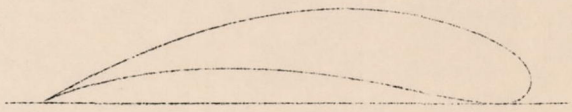
Lift coefficient, drag coefficient and moment about leading edge, also of normal force plotted against α for a conventional wing having a profile conformably to Fig.2.



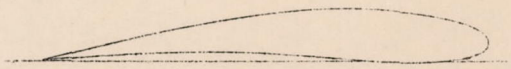
Center of top side of all sections



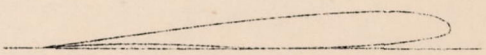
Göttingen 544 1 & 2, $\frac{f}{l}$ = 0.300 $\frac{d}{l}$ = 0.150



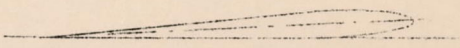
Göttingen 577 3, $\frac{f}{l}$ = 0.210 $\frac{d}{l}$ = 0.135



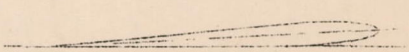
Göttingen 580 4, $\frac{f}{l}$ = 0.075 $\frac{d}{l}$ = 0.095



Göttingen 429 5, $\frac{f}{l}$ = 0.020 $\frac{d}{l}$ = 0.070



Göttingen 537 6, $\frac{f}{l}$ = 0 $\frac{d}{l}$ = 0.050



Göttingen 537 7, $\frac{f}{l}$ = 0 $\frac{d}{l}$ = 0.050

Fig.7 Three-view drawing of No.1 monoplane wing.

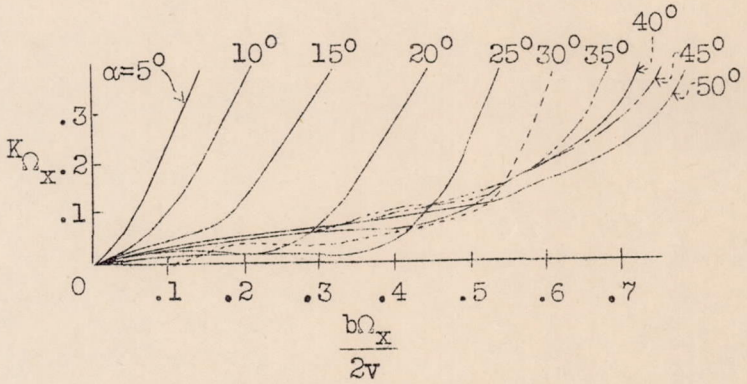


Fig.8 Results of calculation.

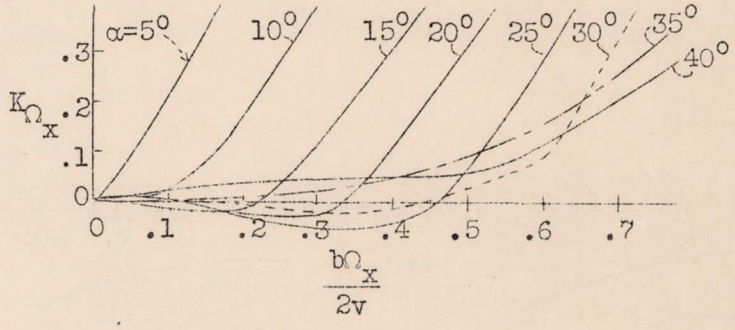


Fig.9 Test data.

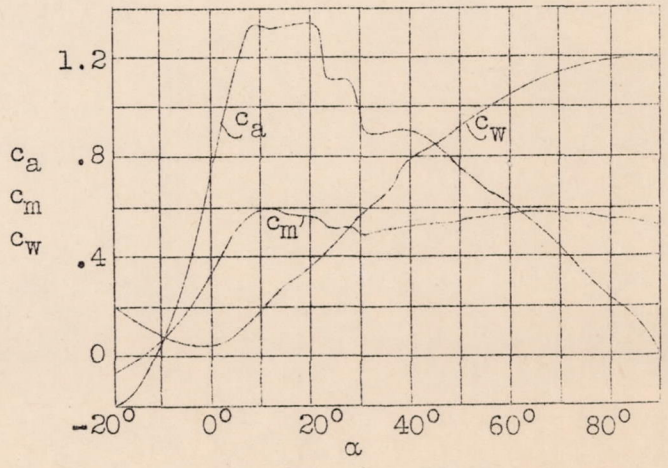


Fig.11 Coefficient of lift, drag and moment about leading edge for wing of Fig.7

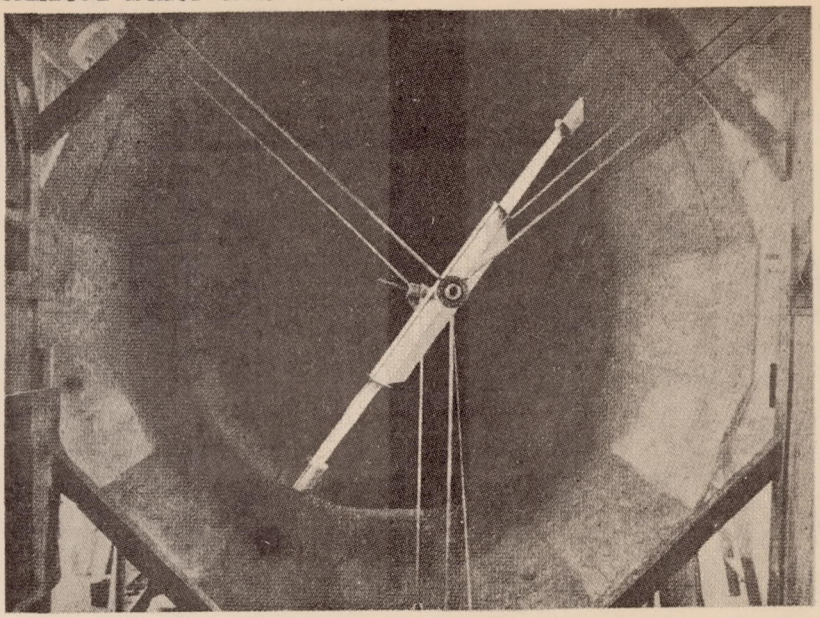


Fig.21 Wing No.2 mounted for autorotation test.

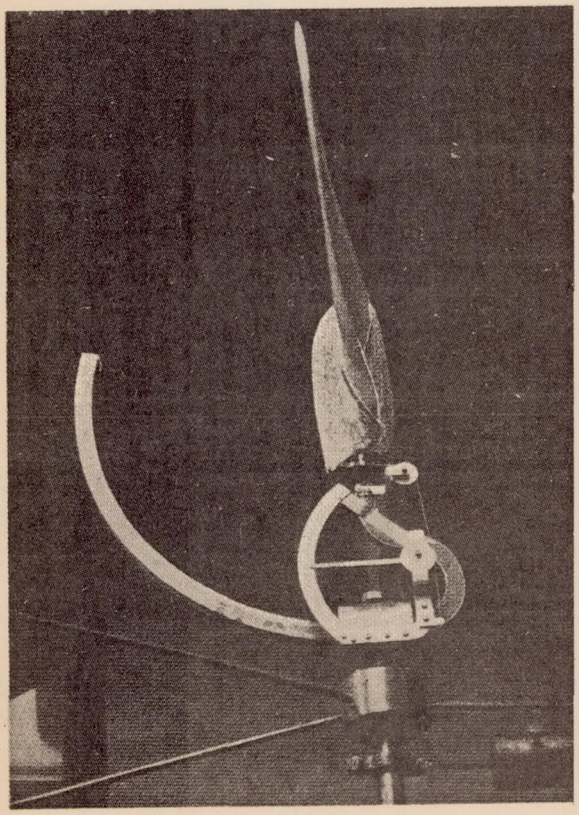


Fig.10 Monoplane wing No.1, mounted on moment balance in Göttingen wind tunnel.

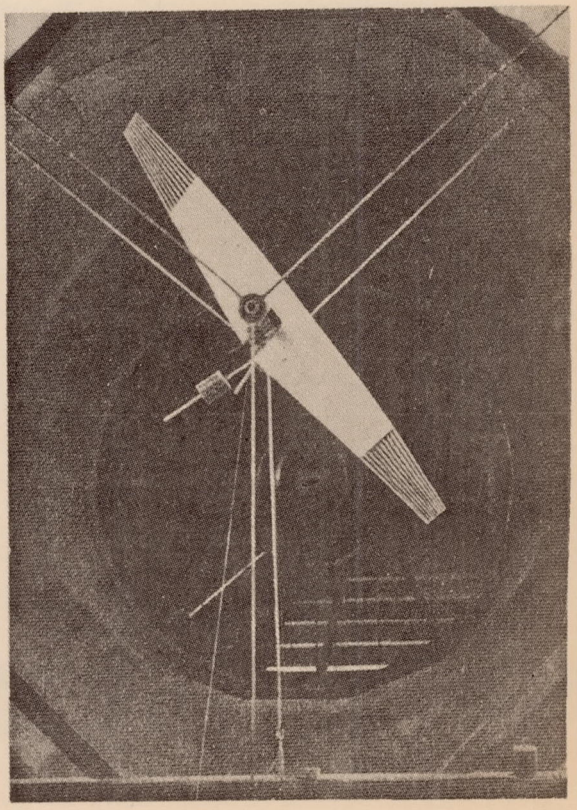


Fig.26 Wing No.3 mounted for autorotation test.

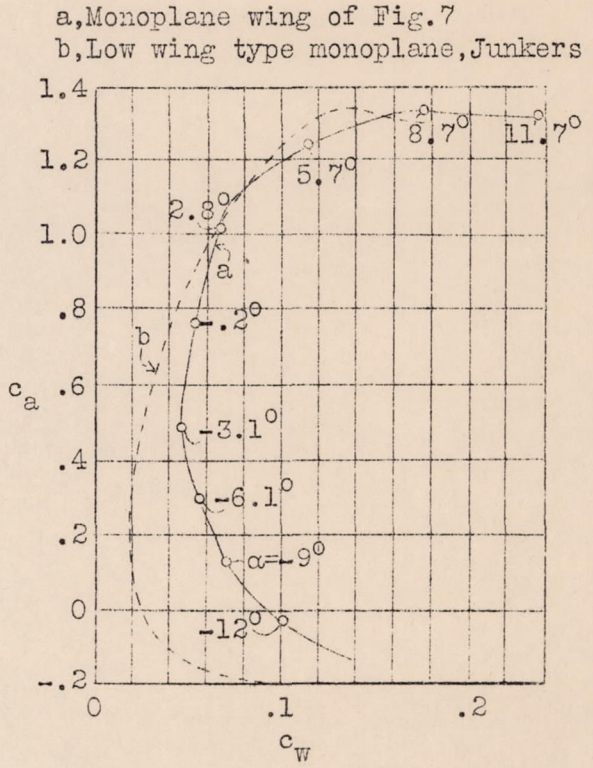


Fig.12 Lift coefficient plotted against drag coefficient.

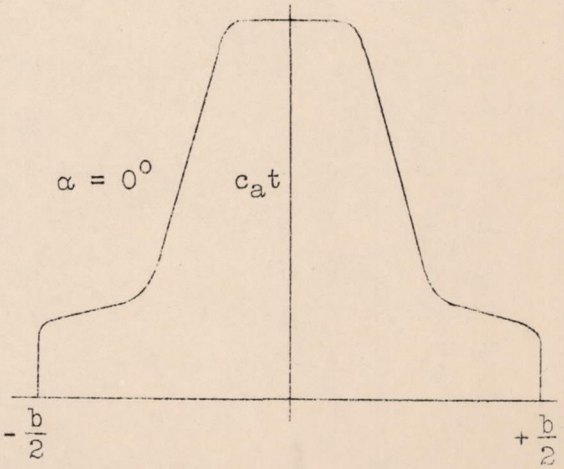


Fig.13 Lift distribution over span of monoplane wing of Fig.7

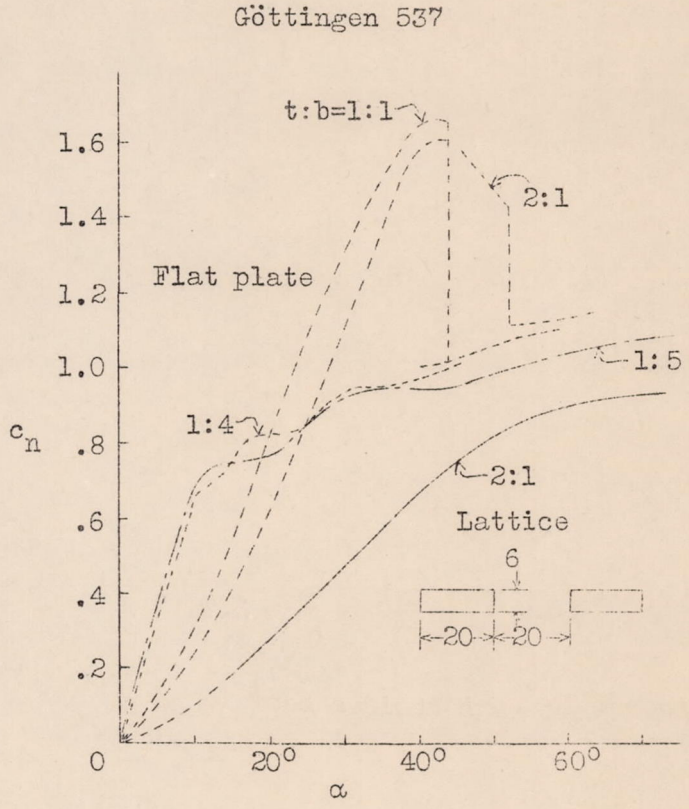


Fig.14 Normal force coefficient plotted against α.

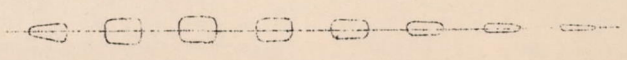


Fig.15 Thin symmetrical interrupted profile.

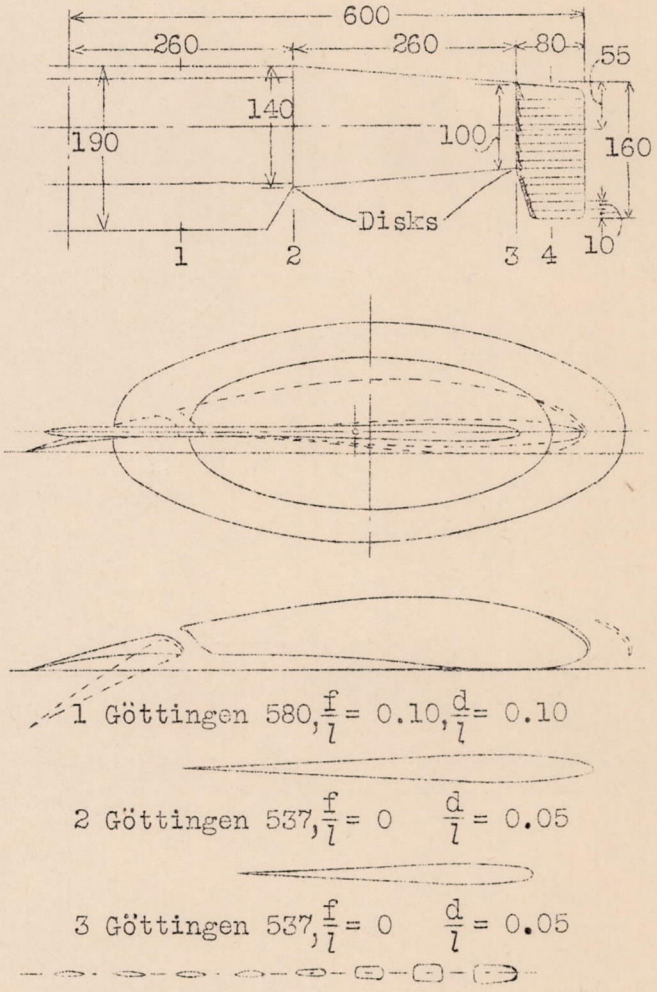
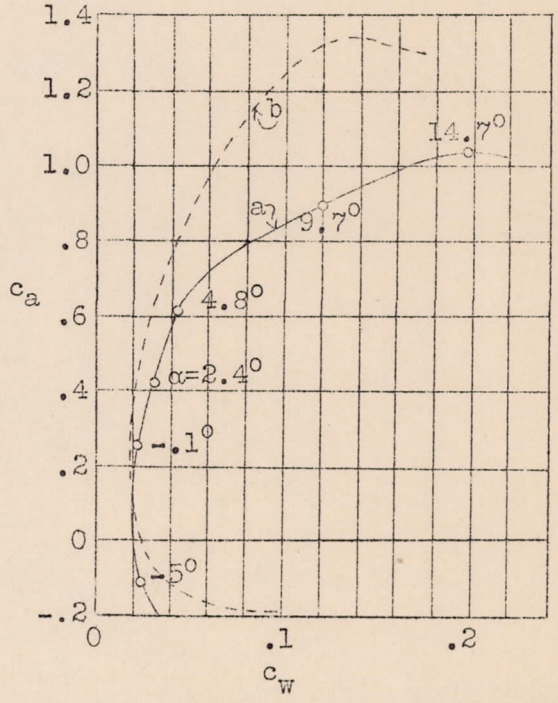


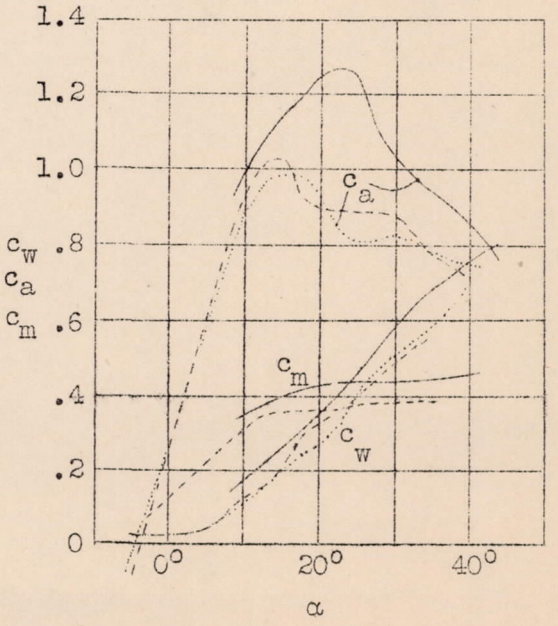
Fig.16 Three-view drawing of monoplane wing No.2



a, Monoplane wing of Fig.16

b, Monoplane wing of type Junkers A35.

Fig.17 Lift coefficient plotted against drag coefficient.



Slot closed, flap neutral.

Slot open, flap turned down 20°.

Calculated according to equation (2).

Fig.18 Coefficient of lift, drag and moment about leading edge for monoplane wing of Fig.16.

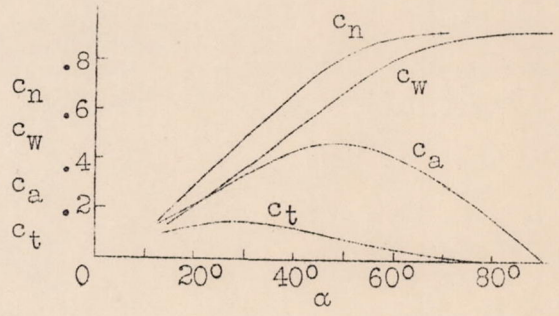


Fig.19 Coefficients of lift, drag, normal and tangential force of a lattice 1 m thick and 0.5 m wide with profile partially shown in Fig.14.
(1 meter = 3.28 ft.)

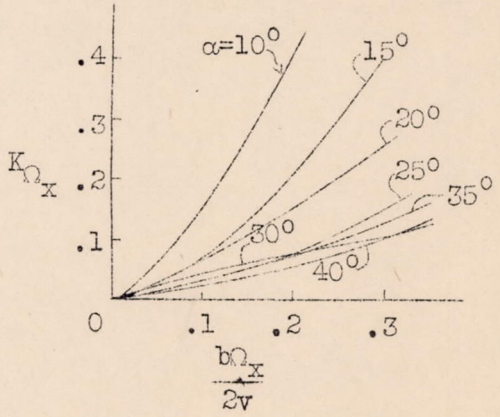
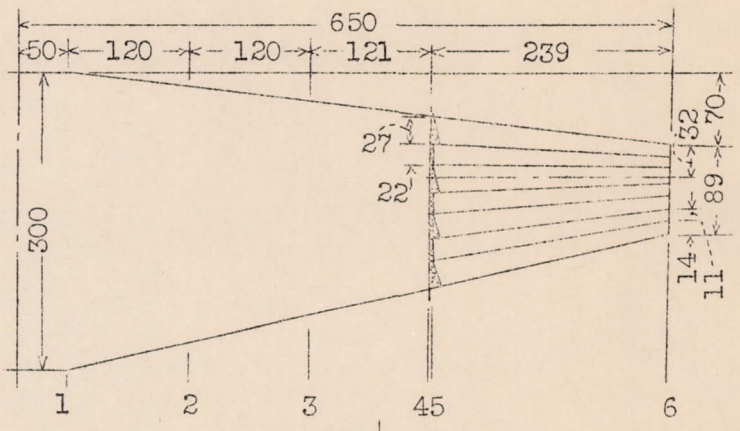
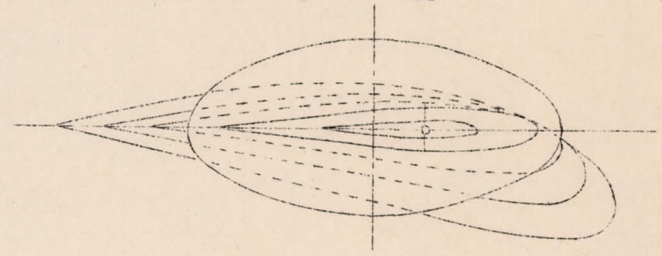


Fig.20 Coefficient of moment about longitudinal axis plotted against $\frac{b\Omega_x}{2v}$, angle α as parameter for monoplane wing of Fig,16.

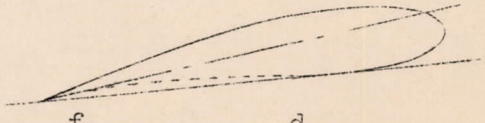




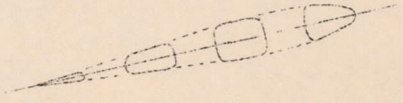
1, $\frac{f}{l}$ = 0.15 $\frac{d}{l}$ = 0.20



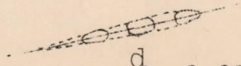
2, $\frac{f}{l}$ = 0.10 $\frac{d}{l}$ = 0.17



3, $\frac{f}{l}$ = 0.05 $\frac{d}{l}$ = 0.14



4 &5, $\frac{f}{l}$ = 0 $\frac{d}{l}$ = 0.11



6, $\frac{f}{l}$=0 $\frac{d}{l}$ = 0.05

Fig.22 Three-view drawing of wing No.3

a, Monoplane wing of Fig.22

b, Monoplane wing type Junkers A35.

c, Without interrupted wing tips.

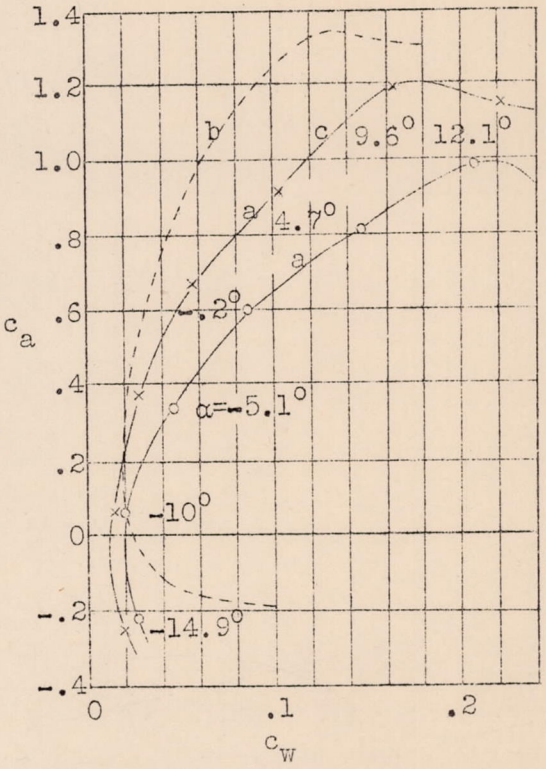


Fig.23 Lift coefficient plotted against drag coefficient.

a, Without underbroken wing tips.

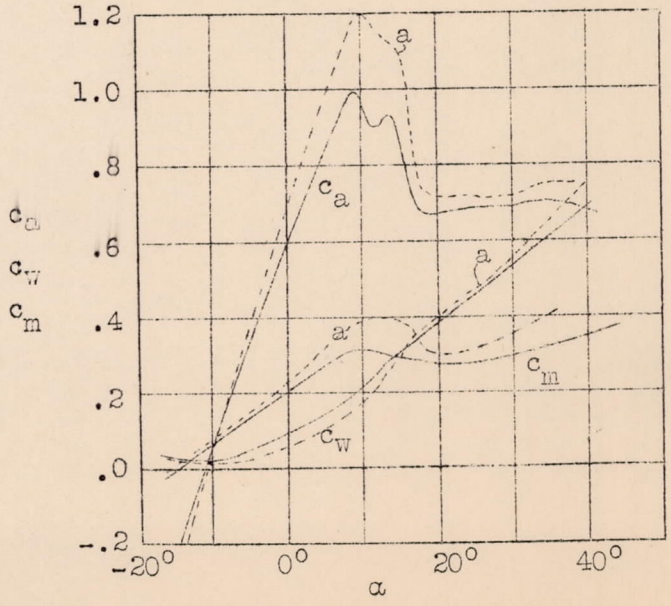


Fig.24 Coefficients of lift, drag and moment about leading edge plotted against α for wing of Fig.22.

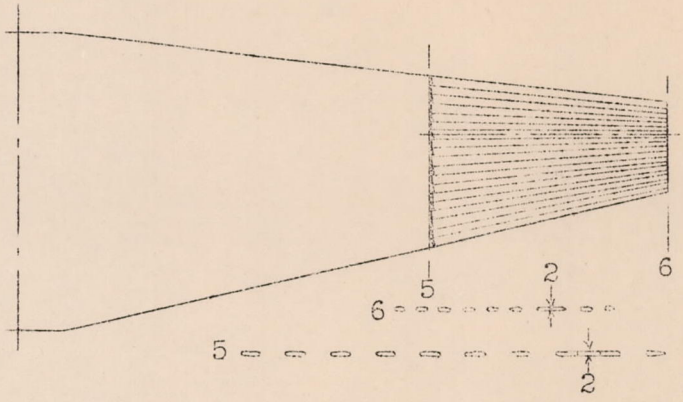


Fig.25 Monoplane wing of Fig.22 with modified tips.

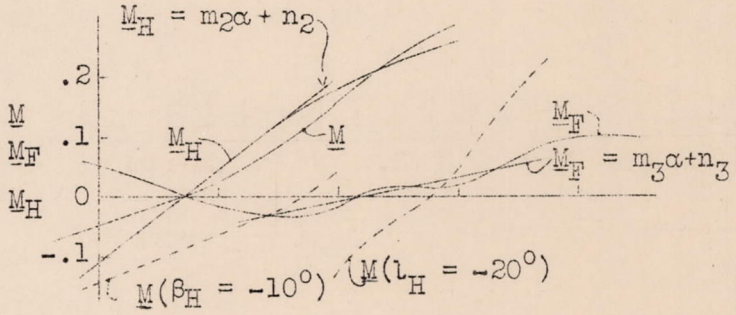


Fig.27 Coefficients of airplane moment, wing moment and elevator moment about lateral axis plotted against α for monoplane, type Junkers A35.

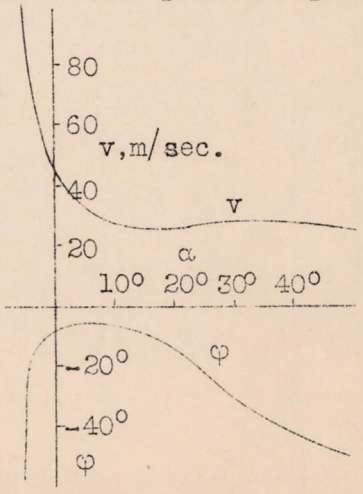


Fig.28 Glide angle and rate of glide plotted against α.

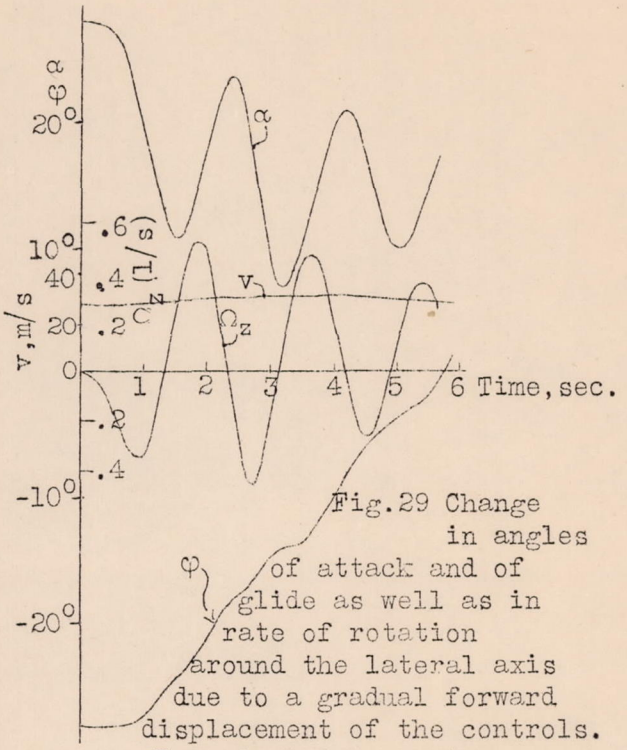


Fig.29 Change in angles of attack and of glide as well as in rate of rotation around the lateral axis due to a gradual forward displacement of the controls. Numerical integration.

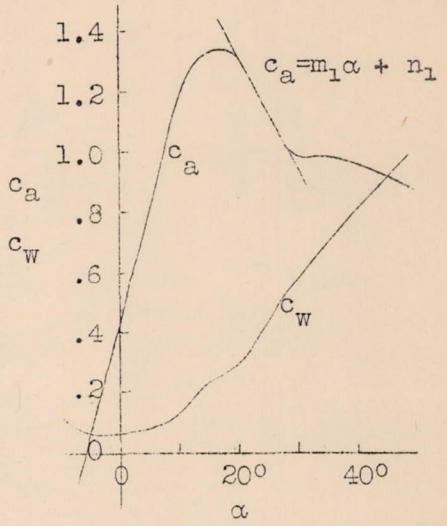


Fig.30 Coefficients of lift and drag plotted against α for a low wing monoplane of type Junkers A 35.

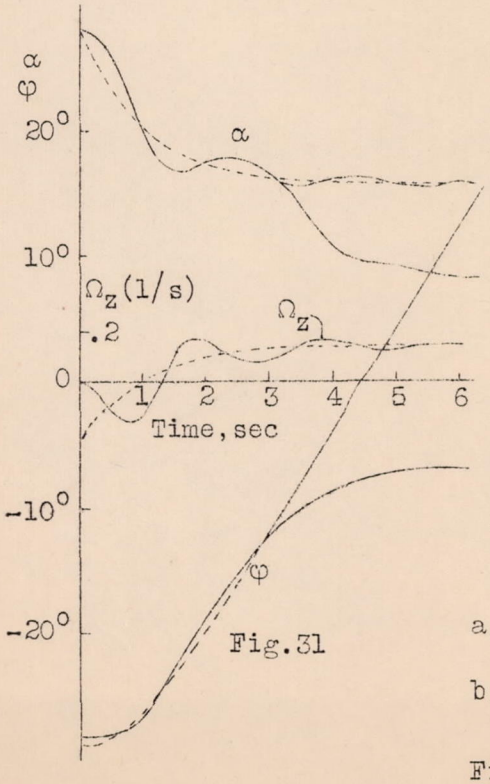
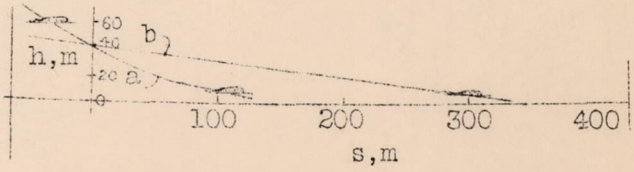


Fig.31

Fig.31 Change in angles of attack of glide and in rate of rotation about the lateral axis due to gradual forward displacement of controls.



a, With non-autorotating wing and horizontal tail surfaces rotatable as one unit.
b, With ordinary wing and ordinary horizontal tail surfaces.

Fig.32 Landing of a low wing monoplane of type Junkers A 35. Height of landing plotted against taxing run.